

# Geometric Phase Gates via Adiabatic Control Using Electron Spin Resonance

Hua Wu,<sup>1</sup> Erik M. Gauger,<sup>1,2</sup> Richard E. George,<sup>1</sup> Mikko Möttönen,<sup>3,4</sup> Helge Riemann,<sup>5</sup> Nikolai V. Abrosimov,<sup>5</sup> Peter Becker,<sup>6</sup> Hans-Joachim Pohl,<sup>7</sup> Kohei M. Itoh,<sup>8</sup> Mike L. W. Thewalt,<sup>9</sup> and John J. L. Morton<sup>10,11,\*</sup>

<sup>1</sup> *Department of Materials, Oxford University, Oxford, OX1 3PH, UK*

<sup>2</sup> *Centre for Quantum Technologies, National University of Singapore, 3 Science Drive 2, Singapore 117543*

<sup>3</sup> *Department of Applied Physics, Aalto University, P.O. Box 14100, FI-00076 AALTO, Finland*

<sup>4</sup> *Low Temperature Laboratory, Aalto University, P.O. Box 13500, FI-00076 AALTO, Finland*

<sup>5</sup> *Leibniz-Institut für Kristallzüchtung, 12489 Berlin, Germany*

<sup>6</sup> *PTB Braunschweig, 38116 Braunschweig, Germany*

<sup>7</sup> *VITCON Projectconsult GmbH, 07743 Jena, Germany*

<sup>8</sup> *School of Fundamental Science and Technology, Keio University, Yokohama, Japan*

<sup>9</sup> *Department of Physics, Simon Fraser University, Burnaby, BC, Canada*

<sup>10</sup> *Department of Materials, Oxford University, Oxford, OX1 3PH, UK*

<sup>11</sup> *Present address: London Centre for Nanotechnology, University College London, 17-19 Gordon St, London WC1H 0AH*

(Dated: December 3, 2024)

High fidelity quantum operations are a key requirement for fault-tolerant quantum information processing. In electron spin resonance, manipulation of the quantum spin is usually achieved with time-dependent microwave fields. In contrast to the conventional dynamic approach, adiabatic geometric phase operations are expected to be less sensitive to certain kinds of noise and field inhomogeneities. Here, we investigate such phase gates applied to electron spins both through simulations and experiments, showing that the adiabatic geometric phase gate is indeed inherently robust against inhomogeneity in the applied microwave field strength. While only little advantage is offered over error-correcting composite pulses for modest inhomogeneities, the adiabatic approach reveals its potential for situations where field inhomogeneities are unavoidably large.

Precise coherent control of quantum systems is an essential ingredient for many quantum technologies. In particular, high fidelity gate operations on quantum bits (qubits) are central to practical realisations of quantum information processing [1]. The electron spin provides a well-defined two-level system that is well-suited for the physical implementation of a qubit. Dynamic control of electron spin states is commonly realized by applying microwave pulses in electron spin resonance (ESR) [2]. Although single microwave pulses in conventional ESR spectrometers usually have non-negligible errors in amplitude and phase [3], high fidelity single qubit operations can often still be realized using carefully designed composite pulses such as BB1 pulses [4, 5] and Knill pulses [6, 7].

A different approach to qubit operations involves geometric manipulations of the quantum system [8–11]. This geometric approach to quantum computing is argued to be more robust against noise in the control parameters [12, 13]. Geometric single- and two-qubit logic gates have been demonstrated in some systems such as nuclear spins [14–16], trapped ions [17] and superconducting qubits [18, 19]. For spin 1/2 systems, theoretical calculations predict robustness against fluctuations in the static field and inhomogeneities in the microwave field [20]; and this has also been explored experimentally with trapped ultracold neutrons [21].

Here, we demonstrate the implementation of a single qubit geometric phase gate via adiabatic passage for electron spins. We show that under current experimental conditions this leads to a much higher fidelity than for a simple dynamic phase gate. Interestingly, we find the adiabatically obtained fidelity is comparable to a geometric phase gate using composite dynamic pulses. These results are also verified by simulations,

which also allow us to extrapolate that the fidelity of the adiabatic geometric phase gate remains high when the inhomogeneity in the microwave field strength becomes larger, unlike for the dynamic approach.

After a cyclic evolution, a quantum system acquires a phase that depends only on the geometric property of the evolution, the so-called Berry phase [8]. For an electron spin 1/2, this geometric phase is determined by its trajectory on the Bloch sphere. Consider a spin initialised in the eigenstate  $|0\rangle$  with respect to a static magnetic field along the  $z$ -axis, and with an additionally applied microwave field detuned from resonance (see Fig. 1 A). Then, slowly tuning the microwave frequency into resonance induces the eigenstate  $|0(t)\rangle$  to follow the effective magnetic field  $B(t)$  adiabatically, rotating it into the  $xy$ -plane. The phase of the microwave can now be swept to rotate the spin's eigenstate by some angle  $\phi$ . Finally, the microwave field is detuned again, taking the eigenstate back to the  $z$ -axis. The geometric phase  $\gamma_{|0\rangle}$  acquired by the state  $|0\rangle$  is given by the enclosed solid angle  $\Theta$  of its trajectory on the Bloch sphere,  $\gamma_{|0\rangle} = \Theta/2 = \phi/2$ . By the same analysis, the geometric phase acquired for the  $|1\rangle$  state is  $\gamma_{|1\rangle} = -\phi/2$ , yielding a geometric phase for general state of  $\gamma = \gamma_{|0\rangle} - \gamma_{|1\rangle} = \phi$ .

In addition to the geometric phase, the electron spin also acquires a dynamic phase during the evolution given by  $\delta = \int_0^\tau \frac{1}{\hbar} g\mu B(t) \cdot S dt$ , where  $\tau$  is the total length of the control sequence.  $S$  is the usual spin operator, so that  $g\mu B(t) \cdot S = E(t)$  is the time-dependent energy of the eigenstate. To remove this dynamic phase from the final state, we introduce a  $\pi$  phase shift of the microwave field exactly halfway through the control sequence. The dynamic phase accumulated dur-

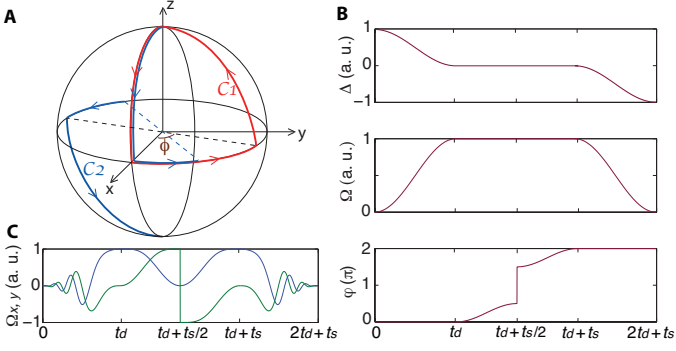


FIG. 1: **A:** Evolution of the spin eigenstate  $|0\rangle$  (red trace  $C_1$ ) and effective magnetic field arising from the applied microwave field (blue trace  $C_2$ ). **B:** The detuning  $\Delta$ , amplitude  $\Omega$  and phase  $\varphi$  of the microwave field during an adiabatic  $\pi$  phase gate. The microwave frequency is tuned from off-resonance to resonance between time 0 and  $t_d$  and then kept resonant for a period of  $t_s$  while the phase  $\phi$  of the microwave is swept. After time  $t_d + t_s$  the microwave is detuned again. The effective field changes sign after the  $\pi$  phase shift at  $t_d + t_s/2$ . **C:** The  $x$  (blue) and  $y$  (green) components of the microwave field applied to the electron spin for a  $\pi$  phase gate.

ing the second half of the control sequence then is  $\delta_2 = \int_{t_d+t_s}^{t_d+t_s/2} \frac{1}{\hbar} g\mu B(t) \cdot S dt = -\int_0^{t_d+t_s/2} \frac{1}{\hbar} g\mu B(t) \cdot S dt = -\delta_1$ , thus cancelling out the final dynamic phase component.

There are two options for tuning the initially off-resonant microwave field into resonance: first, by adding an offset to the static field  $B_0$  field in  $z$ -direction whose magnitude decreases in time. Second, by tuning the microwave field itself via frequency modulation. As the length of the adiabatic process is within a few microseconds, this latter approach is easier than varying a static magnetic field on this timescale.

For a time-dependent microwave frequency  $\omega(t)$ , the transformation of the Hamiltonian from the lab frame to a rotating frame with subsequent rotating wave approximation (RWA) can be performed in several ways. For instance, one can use the canonical rotating frame with constant frequency  $\omega_{rf}$ , where the spin's resonance frequency  $\omega_0$  would be a natural choice for  $\omega_{rf}$ . However, the resulting Hamiltonian then features important time-dependent oscillatory terms. Alternatively, we can choose a rotating frame which always tracks the frequency of the driving microwave field  $\omega_{rf} = \omega(t)$ . In this case, the transformed Hamiltonian after the RWA is given by

$$\hat{H} = \begin{pmatrix} \frac{1}{2}(\Delta + t\dot{\Delta}) & \Omega e^{-i\varphi} \\ \Omega e^{i\varphi} & -\frac{1}{2}(\Delta + t\dot{\Delta}) \end{pmatrix}, \quad (1)$$

where  $\Omega, \varphi$  are the (time-dependent) amplitude and phase of the microwave field,  $\Delta = \omega(t) - \omega_0$  is the detuning, and  $\dot{\Delta} = \dot{\omega}(t)$  its time derivative. For our simulations this form of the transformation is used, ensuring that the measurement of the spin magnetization is carried out in the same reference frame that is used for the depiction of the trajectory on the Bloch sphere in Fig. 1 A.

Fig. 1 B and C show an example for a microwave profile

giving rise to an adiabatic geometric  $\pi$  phase gate. The fast oscillations at the beginning and the end of the control sequence in Fig. 1 C arise due to the finite detuning, getting slower as the microwave field approaches resonance ( $\Delta \rightarrow 0$ ), and disappearing entirely for  $t_d \leq t \leq t_d + t_s$ . The variation of  $\Omega_x$  and  $\Omega_y$  during  $t_d \leq t \leq t_d + t_s$  is due to the phase sweep of the microwave which causes the rotation of the spin magnetization in the  $xy$ -plane.

Different choices for the microwave profile can be made, but vitally the time derivatives  $(\dot{\Delta}, \dot{\Omega}, \dot{\varphi})$  must be kept continuous (except at time  $t = t_d + t_s/2$ ) for achieving adiabatic following. However, continuity of the aforementioned parameters is not sufficient for meeting the adiabaticity condition, which also requires that the control sequence should be much slower than the detuned spin precession, i.e.  $\tau \gg \Delta_0^{-1}$ . Both experiment and simulations confirm that with all the other parameters fixed, the fidelity of the adiabatic phase gate increases with the total length of the adiabatic passage  $\tau$ .

We now simulate such an adiabatic  $\pi$  phase gate and compare its performance with phase gates based on dynamic pulses. The adiabatic implementation is based on the pulse sequence shown in Fig. 1 C, whereas the sequence for applying a dynamic phase  $\phi$  is  $(\frac{\pi}{2})_x - (\phi)_y - (\frac{\pi}{2})_{-x}$ . The corresponding BB1 composite pulse sequence is built by replacing each single pulse with a composite pulse  $(\theta)_{\varphi_0}(\pi)_{\varphi_1+\varphi_0}(2\pi)_{\varphi_2+\varphi_0}(\pi)_{\varphi_1+\varphi_0}$ , where  $\theta$  and  $\varphi_0$  are the flipping angle and phase of the single pulse,  $\varphi_1 = \arccos(-\theta/4\pi)$ ,  $\varphi_2 = 3\varphi_1$ . It is also possible to construct a dynamic geometric phase gate by applying two  $\pi$  pulses of different phase successively  $(\pi)_{\varphi_1} - (\pi)_{\varphi_2}$ , and the BB1 version of this sequence can be built accordingly. The geometric phase acquired by this operation is determined by the phase difference between the two  $\pi$  pulses:  $\gamma = 2(\varphi_2 - \varphi_1)$ .

The simulated phase errors of the three different phase gates are plotted as a function of the deviation from a given microwave amplitude (Fig. 2 A). The maximum deviation  $\Delta\Omega_0$  from its center value  $\Omega_0$  is set to  $\pm 10\%$ , a common value for typical ESR spectrometers. The results show that the phase error in the BB1 dynamic phase gate is much larger than for both geometric phase gates. The relative phase error has a third order dependence on the error in microwave amplitude for the BB1 dynamic phase gate, i.e.  $\epsilon_{r,dyn} \sim O((\Delta\Omega_0/\Omega_0)^3)$ , whereas it has a sixth order dependence for the BB1 geometric phase gate, i.e.  $\epsilon_{r,geo} \sim O((\Delta\Omega_0/\Omega_0)^6)$ . The relative phase error in the adiabatic geometric phase gate is comparable with the BB1 geometric phase gate in this range of microwave inhomogeneity. However, we can see that if the microwave field strength inhomogeneity becomes larger than 10%, which is the case for most coplanar cavities, the performance of the adiabatic phase gate is better than that of the BB1 geometric phase gate. Small fluctuations of the adiabatic gate are due to imperfect adiabaticity of the operation, decreasing both for a stronger microwave field or a slower passage.

The quality of a phase gate can also be characterised by the

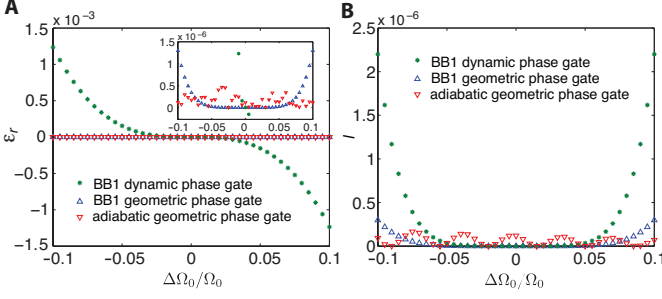


FIG. 2: **A**: The relative phase errors  $\epsilon_r = \gamma/\pi - 1$  of an adiabatic geometric  $\pi$  phase gate, dynamic and geometric  $\pi$  phase gates using BB1 pulses as a function of the error in microwave amplitude  $\Delta\Omega_0/\Omega_0$ . **B**: The infidelity of the phase gate operations as a function of  $\Delta\Omega_0/\Omega_0$ . All simulations involve a single spin 1/2 and do not include spin packet effects. The parameters are  $\Omega_0 = 5$  G, initial detuning  $\Delta_0 = 6$  MHz,  $t_d = 2$   $\mu$ s,  $t_s = 4$   $\mu$ s.

infidelity  $I$  of the operation, defined as

$$I = 1 - \frac{|\text{Tr}[UU_0^{-1}]|}{2}, \quad (2)$$

where  $U_0$  and  $U$  are the operators for an idealized and simulated  $\pi$  phase gate, respectively. Fig. 2 **B** shows the infidelity of the three phase gates as a function of  $\Delta\Omega_0/\Omega_0$ . For the two phase gates using BB1 composite pulses, the infidelity increases as  $O((\Delta\Omega_0/\Omega_0)^6)$ . The infidelity of the BB1 dynamic phase gate is much smaller than its phase error, because in the measurement of infidelity only the diagonal elements of  $U$  are considered while the phase error  $\epsilon_r$  is more directly related to the off-diagonal elements of  $U$ . The oscillations in the infidelity of the adiabatic phase gate are due to the finite non-adiabaticity of the operation, but only have a minor effect on the geometric phase. Once again, the infidelity of the BB1 geometric gate is comparable with the adiabatic variant within  $\pm 10\%$  microwave inhomogeneity, yet the adiabatic phase gate is more robust when the inhomogeneity becomes larger.

In the experiment, we used a sample with narrow ESR linewidth (P donors in high-purity  $^{28}\text{Si}$  crystal at 8K) in order to ensure that all the spins are within the bandwidth of the adiabatic control sequence. The X-band microwave signal is generated at a constant frequency, which is then modulated by the  $I/Q$  signals from an arbitrary waveform generator to create the required microwave field, such as the one shown in Fig. 1 **C**. The complete sequence for measuring the geometric phase gate consists of an initial (dynamic)  $\pi/2$  pulse that creates the spin coherence in the  $xy$ -plane, the adiabatic control sequence, and a (dynamic)  $\pi$  pulse that refocuses the random field inhomogeneities in the environment (Fig. 3 **A** inset). The spin echo is detected and its phase is determined by quadrature detection, from which the phase acquired by the electron spin during the adiabatic phase gate can be deduced.

Fig. 3 **A** shows the phase of the electron spin  $\gamma$  measured after an adiabatic phase gate that is designed to apply a geometric phase  $\phi$  to the spin, and the corresponding error defined

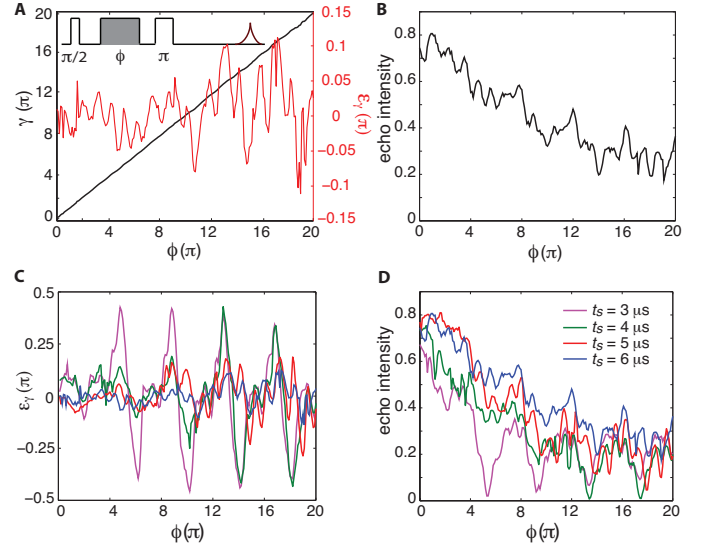


FIG. 3: **A**: Geometric phase  $\gamma$  (black) and the error  $\epsilon_\gamma$  (red) measured as a function of the angle  $\phi$  that the spin rotates in the  $xy$  plane during the adiabatic sequence. Inset: Pulse sequence for measuring the geometric phase gate. **B**: Intensities of the measured spin echo signal normalized to the echo intensities of a Hahn echo at the same position. **C**: Phase error and **D**: echo intensity for adiabatic phase gates of different  $t_s$ . In these experiments  $t_d = 2$   $\mu$ s, maximum of the microwave amplitude  $\Omega_0 = 0.23$  G, initial detuning  $\Delta_0 = 6$  MHz.

as  $\epsilon_\gamma = \gamma - \phi$ . The experimental data follows the theoretical relation  $\gamma = \phi$  very well over a broad range of  $\phi$ , from 0 to  $20\pi$ , which verifies that we have successfully implemented the adiabatic geometric phase gate to the electron spins. The intensity of the spin echo is also plotted against  $\phi$  (Fig. 3 **B**) as a measurement of the performance of the phase gate. The echo intensities are normalized to a Hahn echo detected at the same position. The fact that the echo intensity at  $\phi = 0$  is less than 1 indicates that the adiabatic process is not perfect, and implies only partial adiabatic following of the whole spin ensemble. This is partly due to the off-resonance error of the spins, however, since the ESR linewidth of the spins is narrower than the bandwidth of the adiabatic control sequence, the failure of adiabatic following is more generally due to the non-adiabaticity of the phase gate operation. This also explains why the echo intensity decreases for greater  $\phi$ : for a fixed duration of the adiabatic sequence; a greater  $\phi$  implies a faster phase variation in the  $xy$  plane during  $t_d < t < t_d + t_s$ , hence a less adiabatic operation. In addition, because of the off-resonance error and inhomogeneities in the microwave field, different spin packets do not follow exactly the same path during the adiabatic operation, and by the end of the evolution they will exhibit a spread in the final phase. While the geometric phase  $\gamma$  is a measurement of the mean phase of all the spins, the spin echo intensity reflects the variance of phase of different spin packets, for the reduction of the echo intensity can be understood as due to the loss of phase coherence of the spins.

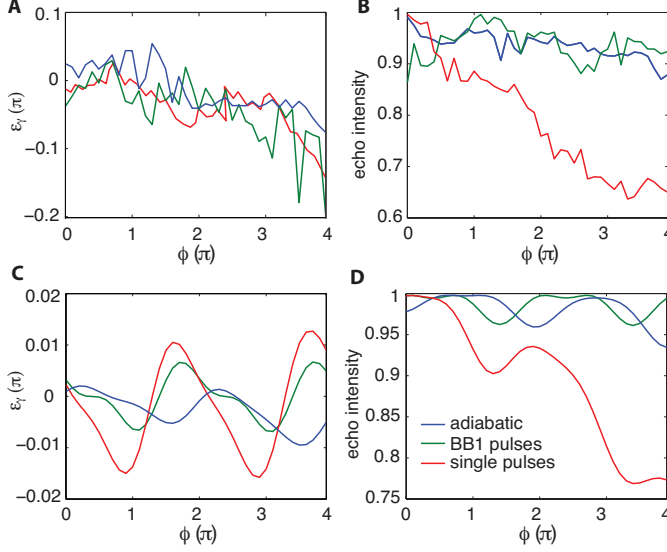


FIG. 4: **A**: Phase error and **B**: echo intensity after an adiabatic geometric phase gate, dynamic phase gates using single microwave pulses and BB1 composite pulses. All the intensities are normalized to 1 in order to compare with the simulation more easily. The parameters used for the adiabatic sequence are the same as in Fig. 3. **C** and **D**: Simulation. The parameters used for the simulation are  $\Omega_0 = 0.5$  G,  $\Delta_0 = 6$  MHz,  $t_d = 2$   $\mu$ s,  $t_s = 4$   $\mu$ s.

The effect of varying  $t_s$ , which determines the sweep rate of  $\phi$  in the  $xy$  plane, is shown in Fig. 3 **C**, **D**. In accordance with the adiabatic condition, the phases measured with shorter  $t_s$  contain larger errors. Meanwhile, the echo intensity reduces more quickly for shorter  $t_s$  which means the adiabatic following is worse. The dips in the echo intensity traces for  $t_s = 3$   $\mu$ s and  $4$   $\mu$ s are attributed to the non-adiabaticity of the phase gate rather than noise from the spectrometer, as we have observed similar features in simulations where the only imperfection introduced is the microwave field inhomogeneity.

We now compare the adiabatic phase gate to a dynamic phase gate effected by single microwave pulses and composite pulses. The gates are studied over the range of  $[0, 4\pi]$  since the definition of the BB1 pulse is limited to  $4\pi$  and the geometric phase gate using dynamic pulses can only apply a phase of less than  $4\pi$ . The pulse sequences for the dynamic gates are as described above for the simulations. Limited by the output level of the signal generator and the range of linear amplification of the spectrometer and solid-state amplifier, the maximum amplitude of the microwave field we can apply is about 0.25 G, corresponding to the length of a  $\pi$  pulse  $\tau_\pi = 700$  ns. In this case the BB1 pulse sequence for a dynamic  $\pi$  phase gate is  $14 \times \tau_\pi = 9.8$   $\mu$ s, therefore we choose  $t_s = 6$   $\mu$ s and  $t_d = 2$   $\mu$ s for the adiabatic sequence so that its total length  $\tau = 10$   $\mu$ s is comparable with the BB1 pulse sequence.

The measured phase as well as the echo intensity show that the adiabatic phase gate works better than the dynamic phase

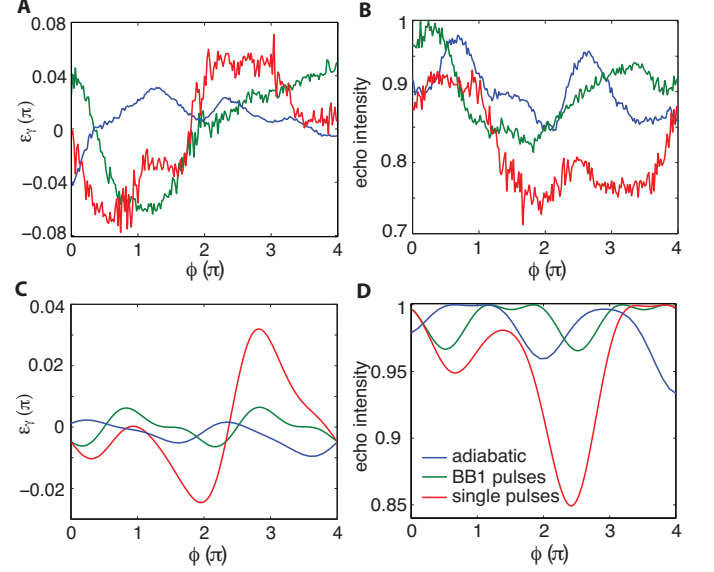


FIG. 5: **A**: Phase error and **B**: echo intensity after an adiabatic geometric phase gate, geometric phase gates using single microwave pulses and BB1 composite pulses. **C** and **D**: Simulation. The parameters for the simulation are the same as the one used for Fig. 4 **C** and **D**.

gate using single microwave pulses (Fig. 4, 5 **A** and **B**), but it has a comparable performance to the dynamic gates using BB1 composite pulses. The comparison between the experimental data and simulations (Fig. 4, 5 **C** and **D**) also verifies that the adiabatic geometric phase gate is more robust under  $B_1$  inhomogeneity. In all the simulations we assumed 10% inhomogeneity in  $B_1$  and no off-resonance effect. In Fig. 4 **D** the simulation reproduces the main features in the echo intensity of the dynamic phase gate using single pulses (red trace), which implies that the decrease in the echo intensity are essentially due to the  $B_1$  inhomogeneity.

From the point of view of decoherence, a previous theoretical study has suggested that the slow adiabatic process would suffer from the decoherence from the environment and thus does not have real advantage over the dynamic gate operations [22]. Although in our experiment the gate time for the BB1 phase gate is similar to that of the adiabatic gate, the fidelity of the adiabatic geometric phase gate is still limited by other imperfections of the equipment such as the small amplitude of the microwave field and phase imprecision.

In conclusion, we have demonstrated single qubit geometric phase gates using adiabatic control in electron spins. Both experiment and simulation showed that the adiabatic geometric phase gate is robust against inhomogeneities in the microwave field. The performance of the adiabatic geometric phase gate should improve with a larger amplitude microwave field, for example achieved using a higher Q-factor resonator [23]. For the current experimental setup its performance is comparable to the geometric phase gate using composite dynamic pulses such as BB1 pulses. However, the adi-



abatic phase gate could be advantageous given a more inhomogeneous microwave field (such as may arise in coplanar resonators [24]), or at higher microwave amplitudes.

This research is supported by the EPSRC through the Materials World Network (EP/I035536/1), the European Research Council under the European Community's Seventh Framework Programme (FP7/2007-2013) / ERC grant agreement no. 279781, and the National Research Foundation and Ministry of Education, Singapore. HW is supported by KCWong Education Foundation. J.J.L.M. is supported by the Royal Society.

---

\* Electronic address: jjl.morton@ucl.ac.uk

- [1] M. A. Nielsen and I. L. Chuang, *Quantum Computing and Quantum Information* (Cambridge University Press, Cambridge, 2000).
- [2] A. Schweiger and G. Jeschke, *Principles of Pulse Electron Paramagnetic Resonance* (Oxford University Press, 2001).
- [3] J. J. L. Morton, A. M. Tyryshkin, A. Ardavan, K. Porfyakis *et al.*, Phys. Rev. A, **71**, 012332 (2005).
- [4] S. Wimperis, J. Magn. Reson., Ser. A, **109**, 221 (1994).
- [5] J. J. L. Morton, A. M. Tyryshkin, A. Ardavan, K. Porfyakis *et al.*, Phys. Rev. Lett., **95**, 200501 (2005).
- [6] C. A. Ryan, J. S. Hodges and D. G. Cory, Phys. Rev. Lett., **105**, 200402 (2010).
- [7] A. M. Souza, G. A. Álvarez and D. Suter, Phys. Rev. Lett., **106**, 240501 (2011).
- [8] M. V. Berry, Proc. R. Soc. London, Ser. A, **392**, 45 (1984).
- [9] F. Wilczek and A. Zee, Phys. Rev. Lett., **52**, 2111 (1984).
- [10] Y. Aharonov and J. Anandan, Phys. Rev. Lett., **58**, 1593 (1987).
- [11] S.-L. Zhu and Z. D. Wang, Phys. Rev. Lett., **91**, 187902 (2003).
- [12] A. Ekert, M. Ericsson, P. Hayden, H. Inamori *et al.*, J. Mod. Opt., **47**, 2501 (2000).
- [13] O. Oreshkov, T. A. Brun and D. A. Lidar, Phys. Rev. Lett., **102**, 070502 (2009).
- [14] D. Suter, G. C. Chingas, R. A. Harris and A. Pines, Mol. Phys., **61**, 1327 (1987).
- [15] J. A. Jones, V. Vedral, A. Ekert and G. Castagnoli, Nature, **403**, 869 (2000).
- [16] J. Du, P. Zou, M. Shi, L. C. Kwek *et al.*, Phys. Rev. Lett., **91**, 100403 (2003).
- [17] D. Leibfried, B. DeMarco, V. Meyer, D. Lucas *et al.*, Nature, **422**, 412 (2003).
- [18] P. J. Leek, J. M. Fink, A. Blais, R. Bianchetti *et al.*, Science, **318**, 1889 (2007).
- [19] M. Möttönen, J. J. Vartiainen and J. P. Pekola, Phys. Rev. Lett., **100**, 177201 (2008).
- [20] G. DeChiara and G. M. Palma, Phys. Rev. Lett., **91**, 090404 (2003).
- [21] S. Filipp, J. Klepp, Y. Hasegawa, C. Plonka-Spehr *et al.*, Phys. Rev. Lett., **102**, 030404 (2009).
- [22] A. Nazir, T. P. Spiller and W. J. Munro, Phys. Rev. A, **65**, 042303 (2002).
- [23] T. W. Borneman and D. G. Cory, arXiv:1207.1139.
- [24] H. Malissa, D. I. Schuster, A. M. Tyryshkin, A. A. Houck S. A *et al.*, arXiv:1202.6305v1.